minerals

MDPI

Article

The History of Transgressions during the Late Paleocene-Early Eocene in the Kuqa Depression, Tarim Basin: Constraints from C-O-S-Sr Isotopic Geochemistry

Yang Xu [1,*], Yangtong Cao [2], Chenglin Liu [2,*], Hua Zhang [2] and Xiao Nie [2]

[1] State Key Laboratory of Nuclear Resource and Environment, East China University of Technology, Nanchang 330013, China

[2] MLR Key Laboratory of Metallogeny and Mineral Assessment, Institute of Mineral Resources, Chinese Academy of Geological Sciences, Beijing 100037, China; cyt1941@126.com (Y.C.); zhhcdut@163.com (H.Z.); niexiao369@gmail.com (X.N.)

* Correspondence: 201860042@ecut.edu.cn (Y.X.); liuchengl@263.net (C.L.)

Received: 25 August 2020; Accepted: 21 September 2020; Published: 22 September 2020

Abstract: The Tethys Sea extended into the Kuqa Depression from the Paleocene to the late Eocene and provided an abundant provenance for the deposition of evaporite sequences. Until now, detailed research on the history of transgressions during the late Paleocene-early Eocene in the Kuqa Depression has been limited. Therefore, in this study, we took the upper Paleocene Talak section and the lower Eocene Xiaokuzibai section in the western part of the Depression as the research objects and analyzed the petrology, the carbon and oxygen isotopes of carbonate rocks, and the sulfur and strontium isotopes of gypsum rocks to systematically study the above issues. The $\delta^{13}C$, $\delta^{18}O$ and $\delta^{34}S$ values of the upper Paleocene evaporite sequences were determined to be between 4.2‰ and 5.7‰, between −5.2‰ and 2.4‰, and between 16.5‰ and 17.9‰, respectively. The $\delta^{13}C$, $\delta^{18}O$, $\delta^{34}S$, and $^{87}Sr/^{86}Sr$ values of the lower Eocene evaporite sequences were determined to be between −6.9‰ and −2.0‰, between −9.0‰ and −4.5‰, between 10.5‰ and 17.0‰, and between 0.708642 and 0.709883, respectively. The analysis results show that the evaporite sequence of the upper Paleocene was formed by transgression. The deposition of the evaporite sequence changed from continental to marine deposition, and then gradually transitioned to continental during the Early Eocene. This paper is of great significance for reconstructing the history of transgressions in the Tethys tectonic realm during this period.

Keywords: transgressions; C-O-S-Sr isotopes; late Paleocene-early Eocene; Kuqa Depression

1. Introduction

Multiple transgression-regression cycles of Tethyan seawater occurred during the Cretaceous-Paleogene, and these cycles represent major events during the geological evolution of the Tarim Basin. In the early Cretaceous, seawater invaded from west to east in the southwest of the Tarim Basin, and the transgression scope increased during the Paleocene. Consequently, seawater began to extend into the northern Tarim Basin (the Kuqa Depression) (Figure 1). Therefore, how the transgressions of the late Paleocene-early Eocene affect the Kuqa Depression is an urgent problem that remains to be solved, with obvious significance for revealing the evolution of the Tethyan Sea.

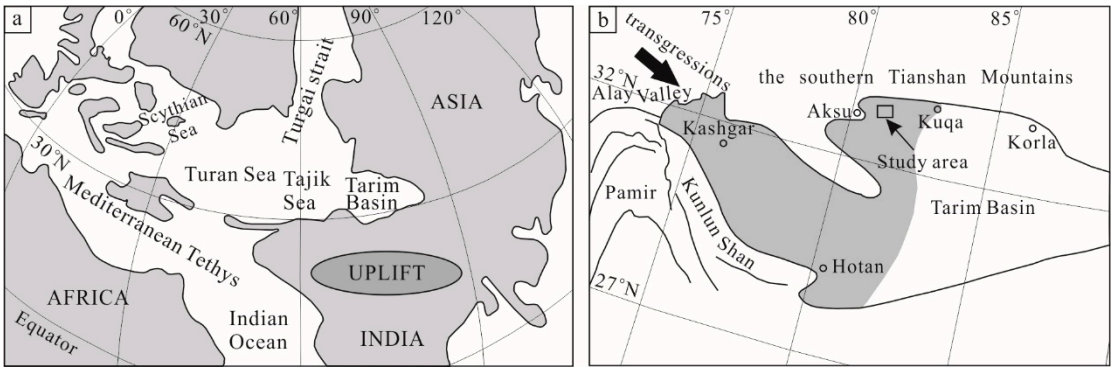

Figure 1. (**a**) Paleogeographic sketch map of the Paleocene and Eocene in the Tethys Realm (modified from Abels et al. 2011 [1]); (**b**) Eocene paleogeographic map of the Tarim Basin (modified from Wang 1985 [2]).

Marine fossils (such as foraminifera, gastropods, and calcareous fossils) have been found in the Paleocene and Eocene strata in this area [3,4]. Fu (1996) and Jia (2002) [5,6] discussed the sedimentary environment by analyzing the spatial distribution and carbon and oxygen isotopic compositions of Paleogene carbonate rocks in the Kuqa Depression. Liu et al. (1987) and Zhang et al. (2013) [7,8] analyzed the provenance based on the sulfur isotopic composition of gypsum from multiple Paleogene stratigraphic sections. Although previous studies on the provenance and sedimentary environments of the evaporite sequences have been conducted, no systematic studies or analyses of typical upper Paleocene-lower Eocene sections have been conducted, especially in terms of the integration of multiple isotope geochemical methods. To some extent, this has affected the ability of researchers to deeply understand and recognize the history of transgressions during the late Paleocene-early Eocene. Therefore, it is of great significance to systematically study the sedimentary environment of the upper Paleocene and lower Eocene strata by combining multiple isotope geochemical methods.

Isotope geochemical proxies can provide valid evidence for explaining the material sources and sedimentary environments of evaporite sequences. The carbon and oxygen isotopic compositions of carbonate rocks are significant paleoenvironmental indicators and can be used to estimate the material sources, paleosalinity, paleotemperature, and other parameters [9–11]. Because sulfur isotope fractionation during gypsum deposition is very weak or even negligible, the sulfur isotopic composition of gypsum is often used to determine the material source during the evaporite deposition period [12,13]. The element strontium does not exhibit isotope fractionation during chemical and biochemical processes, although geological processes, such as evaporation and concentration, can change the concentration of strontium; however, the $^{87}Sr/^{86}Sr$ ratio remains almost constant within a given geological time and sea area [14]. Thus, the strontium isotopic composition can be used as an effective tracer for studying the migration and transition of materials and is often combined with sulfur isotopic compositions to study the material sources [15–18].

Typical Talak and Xiaokuzibai sections of the upper Paleocene and lower Eocene in the Kuqa Depression are the objects of this research, and the C, O, S and Sr isotopic compositions of these evaporite sequences were systematically studied. Then, the provenance and sedimentary environment of the upper Paleocene and lower Eocene carbonate–gypsum sequences in the Kuqa Depression were discussed to reveal the transgression history of the late Paleocene-early Eocene.

2. Geological Setting

The Kuqa Depression is located between the southern Tianshan tectonic belt and the Tarim Basin [19] and features a nearly east-west orientation (Figure 2). It is approximately 410 km long from east to west and approximately 20 to 60 km wide from north to south, with an area of approximately 16,000 km^2. The Hercynian Movement at the end of the early Permian formed the basic appearance of

the basement of the Kuqa Depression [20], and the region then entered the evolution stage of a foreland basin. In the Late Triassic-Early Jurassic, the tectonic setting began to evolve from compressional to extensional. In the Early Cretaceous, the Tarim Basin again featured a compressional tectonic stress field due to the intense collision between the Indian plate and the Eurasian plate [21,22].

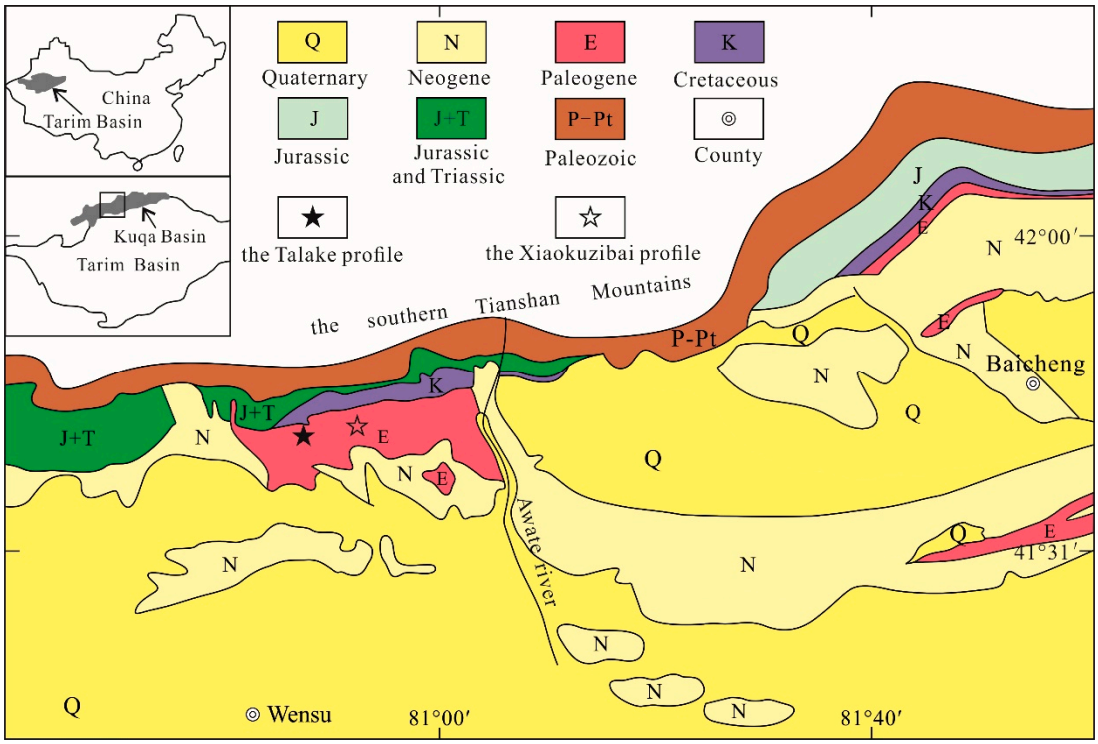

Figure 2. Simplified geological map of the Kuqa Depression and the locations of the Paleocene and Eocene stratigraphic outcrops (modified after the 1:200,000 Geological Map of the Kuqa Depression, 1967).

Five major transgressions affected the development of marine sediments in the Tarim Basin during the Late Cretaceous-Paleogene period [23]. The western part of the Kuqa Depression began to receive seawater at the beginning of the Paleocene, and the key factor controlling the retreat of seawater from the Tarim Basin was mainly the northward growth of the Pamirs rather than the India–Eurasia collision [24,25]. At present, the final phase of seawater retreat from the Tarim Basin occurred mainly between 47 and 33 Ma [26–28]. In this period, thick salt-bearing strata were deposited in the western part of the basin, and the lithology of the Paleocene Talak Formation consists of a succession of thick maroon conglomerate, sandy conglomerate, thin dolomite, mud-bearing gypsum, and silty mudstone from bottom to top. The lower part of the Eocene Xiaokuzibai Formation consists of dark gray silty mudstone, grayish-green silty mudstone, limestone, gypsum and rock salt with dark gray boulder-clay, and the upper part consists of thick rock salt with maroon boulder-clay.

3. Materials and Methods

3.1. Materials

A total of 33 samples were collected for isotope analysis from the upper parts of the Talak Formation and the lower parts of the Xiaokuzibai Formation in the northwestern Kuqa Depression, and each sample was collected at equal intervals (Figure 2). There is no direct and precise dating of the carbonate-gypsum deposition in the Kuqa Depression. However, Zheng and Meng (2006) [29] precisely identified the Paleogene strata age through paleomagnetic data and suggested that the Talak Formation and the Xiaokuzibai Formation formed from 60.5 to 38 Ma. Teng et al. (1997) [30] indicated

that the age of the top boundary of the Xiaokuzibai Formation is 38 Ma based on magnetostratigraphic research of the Cenozoic section of the Kuqa River area. The Paleocene and Eocene samples used in this study are from the Talak Formation and the bottom of the Xiaokuzibai Formation, respectively. Hence, they are inferred to have formed in the late Paleocene and early Eocene, respectively.

The Talak and Xiaokuzibai sections located in the western Kuqa Depression are typical upper Paleocene and lower Eocene sections in the basin, respectively. The Talak section is located in Talak village in the western Kuqa Depression. This section contains evaporite strata deposited in the late Paleocene, which consist of thick maroon conglomerate, thin dolomite, and thick gypsum deposits (Figure 3a–d). Nine dolomite samples and six gypsum samples were collected from the upper Paleocene Talak section (the thickness of the dolomite layer is approximately 1.6 m, and the thickness of the gypsum layer is approximately 13 m). The Xiaokuzibai section is located in the Xiaokuzibai ravine in the western Kuqa Depression. This section contains evaporite strata deposited in the early Eocene, which consist of thick limestone and thick gypsum deposits (Figure 3e,f). Seven carbonate samples and eleven gypsum samples were collected from the lower Eocene Xiaokuzibai section (the thickness of the limestone layer is approximately 9 m, and the thickness of the gypsum layer is approximately 18 m).

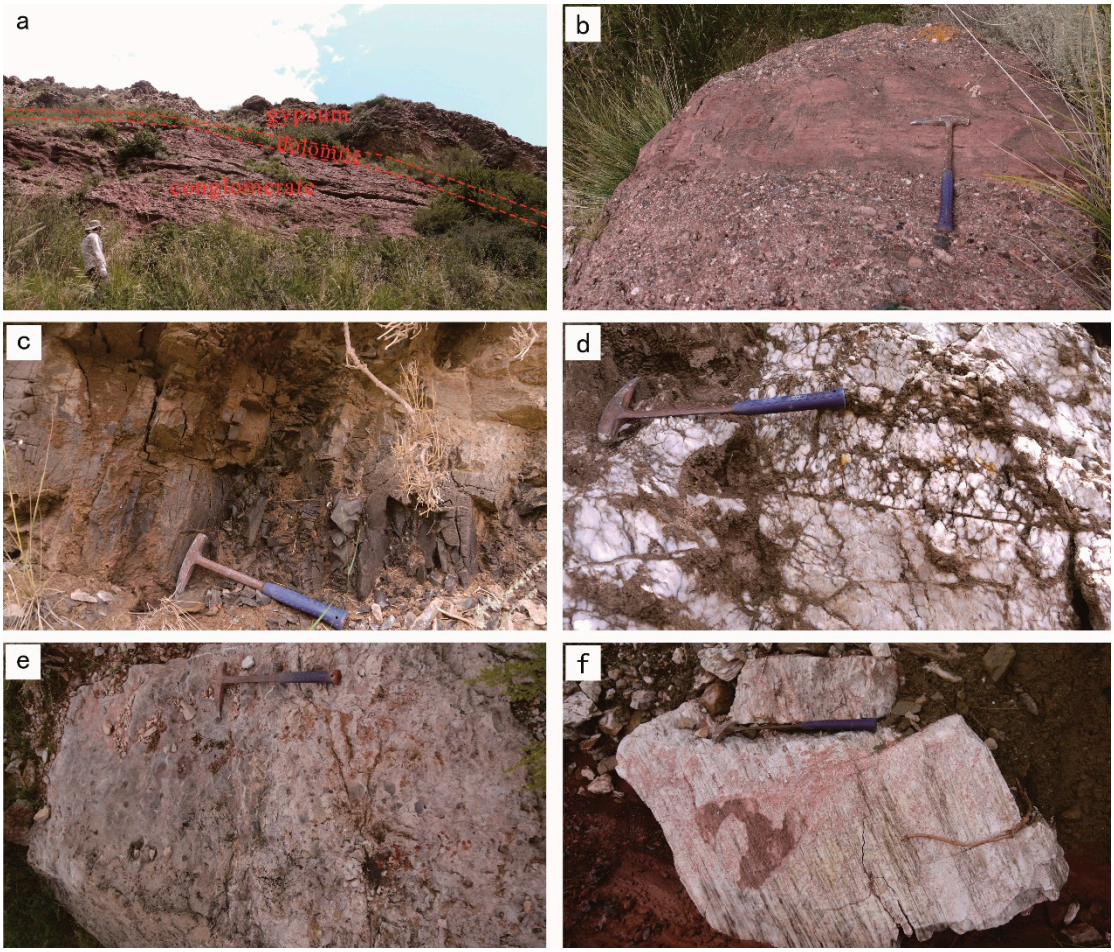

Figure 3. Photographs of the outcrops of upper Paleocene and lower Eocene carbonate-gypsum rock sedimentary sequences. (**a**) upper Paleocene maroon conglomerate, dolomite, and gypsum; (**b**) upper Paleocene conglomerate; (**c**) upper Paleocene dolomite; (**d**) upper Paleocene gypsum; (**e**) lower Eocene limestone; (**f**) lower Eocene laminar gypsum.

The dolomite in the Talak section is muddy dolomite, the hand specimen is dark gray in color, and the appearance is dense and uniform (Figure 4a). Observation under a polarizing microscope showed that the carbonate minerals are dolomite, with a micritic texture and a particle size of generally less

than 5 μm (Figure 4d). These petrographic characteristics show a sedimentary environment with weak hydrodynamic conditions and no terrigenous material supply.

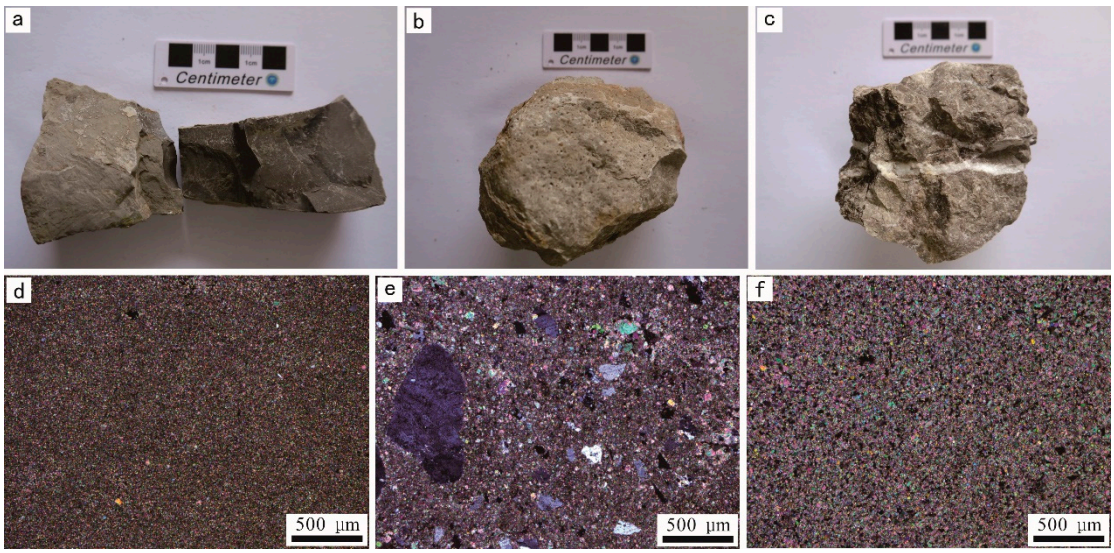

Figure 4. Petrographic characteristics of the upper Paleocene and lower Eocene carbonate rocks. (**a**,**d**): upper Paleocene micritic dolomite; (**b**,**e**): lower Eocene sandy micritic limestone (sample XKZB-02); (**c**,**f**): lower Eocene micritic limestone (sample XKZB-06).

The lower part of the Xiaokuzibai section is sand-bearing micrite, and the upper part is micrite. The hand specimen of the sand-bearing micrite is light brown, and quartz particles are visible to the naked eye (Figure 4b). Observation under a polarizing microscope showed that the minerals mainly include calcite and quartz clasts. The calcite crystals are fine-grained with a micritic texture and a grain size of generally less than 5 μm (Figure 4e). The terrigenous quartz particles are distributed irregularly and chaotically and exhibit angular shapes, low textural maturity, and grain sizes of 50~1200 μm. The hand specimen of the upper micrite is gray, and calcite veins are present in it (Figure 4c). Observation under a polarizing microscope showed that the carbonate minerals are fine-grained calcite with grain sizes of generally less than 7 μm and a micritic texture. Therefore, the lower limestone was deposited in a sedimentary environment characterized by weak hydrodynamic conditions and a terrigenous debris supply; over time, the terrigenous debris supply of the sedimentary environment disappeared.

Fluid inclusions in gypsum are considered to be a source of direct information about primary parent liquor [31]. The upper Paleocene gypsum crystals are mainly characterized by single-phase liquid inclusions with diameters in the range of ~3 to 40 μm (Figure 5a,b). The lower Eocene gypsum crystals are mainly characterized by single-phase liquid inclusions with diameters in the range of ~5 to 50 μm (Figure 5c,d). These inclusions are arranged in planes parallel to the growth zones of gypsum crystals, showing a well-preserved primary texture.

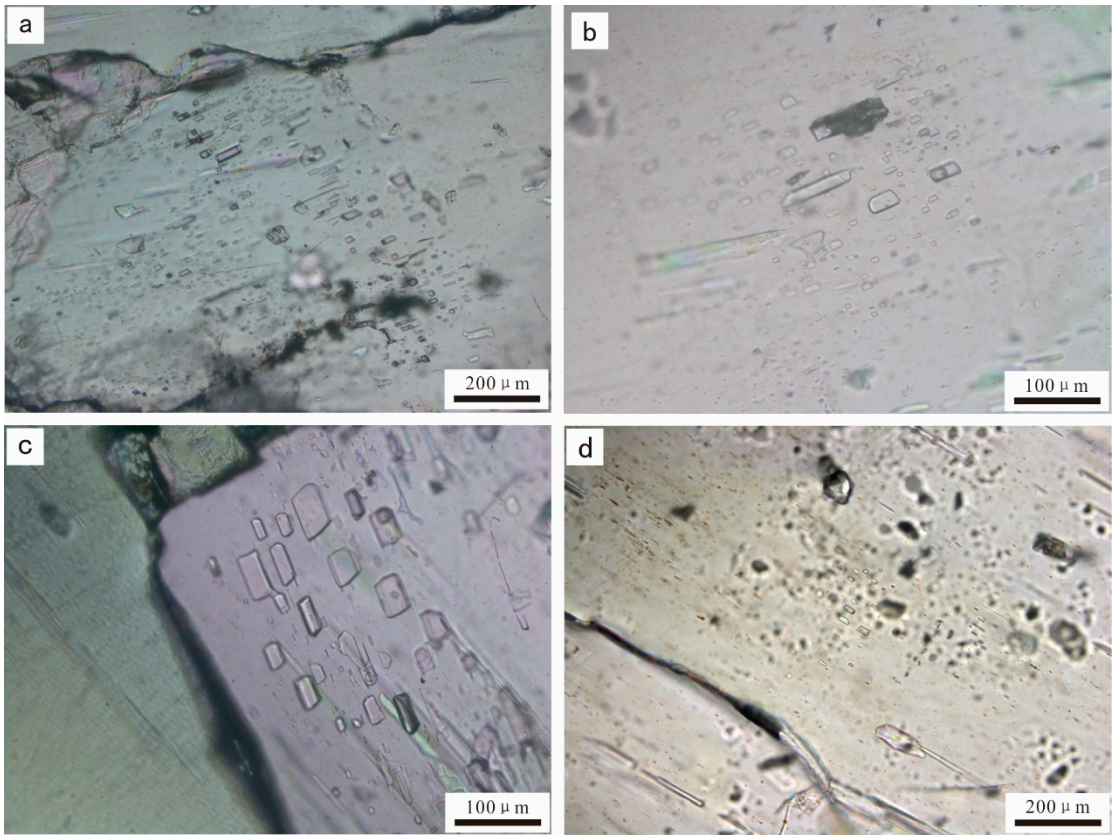

Figure 5. Primary fluid inclusions characteristics of the upper Paleocene (**a**,**b**) and lower Eocene (**c**,**d**) gypsum.

3.2. Experimental Methods

No calcite veins were observed within the upper Paleocene dolomite samples. Some calcite veins were observed in the lower Eocene limestone, so we used an electric drill with a diamond bit to acquire limestone samples from between the veins and observed whether or not there was recrystallization under the microscope. First, the samples were determined to be unaltered before analysis; then, all selected samples were ground to 200 mesh and baked at 110 °C for 3 h. The C and O isotopic compositions and the Mn and Sr contents of the carbonate rocks were measured at the Analytical Laboratory of the Beijing Research Institute of Uranium Geology. The C and O isotopic measurement instrument was a MAT252 mass spectrometer (Finnigan, San Francisco, CA, USA) with an error of less than ±0.2‰. Then, 25 mg were placed at the bottom of the main reaction tube and 5 mL of 100% orthophosphoric acid were poured into the branch tube of the reaction bulb. The two were mixed after vacuumization to react for 16 h with a reaction temperature of 75 °C. Then, a liquid-nitrogen cooled trap (−80 to −70 °C) was used to collect carbon dioxide gas, which was placed into a mass spectrometer for analysis once purified. The standard sample number was GBW04405 and the unit standard was V-PDB. The contents of Mn and Sr were determined by Inductively Coupled Plasma Mass Spectrometry (ICP-MS, Agilent, Palo Alto, CA, USA) with an error of less than ±5%. The samples were first reacted with HCl 5 M to remove carbonate and subsequently dissolved in 18 mΩ cm^{-1} Milli-Q water. To avoid gypsum saturation in the final solution and to ensure a similar range of concentrations, a constant dilution ratio of 1:500 was maintained for all samples. The samples were then filtered through a 0.45 μm cellulose acetate membrane filter to remove any quartz or other insoluble mineral particles.

To prevent other minerals in the original gypsum samples from affecting the effectiveness and accuracy of the test results, we first performed X-ray diffraction analysis on the selected sample before analyzing the sulfur isotopic composition and then selected pure unweathered gypsum to place in an

ultrasonic cleaning machine for 2 times with pure water, then the cleaned samples were dried and crushed to 200 mesh. The S and Sr isotopic compositions were measured at the Institute of Mineral Resources, Chinese Academy of Geological Sciences. The S isotopic measurement instrument was an MAT-251EM mass spectrometer. The sample was purified by Eschka reagent fusion sample into pure $BaSO_4$, and then V_2O_5 oxidant was used to prepare SO_2, and then SO_2 was used for sulfur isotope test and analysis. Based on repeated measurements of the standard sample, the error was less than ±0.1‰, and the results are expressed in δ values relative to the Vienna Canyon Diablo Troilite (V-CDT) standard. The Sr isotopic measurement instrument was a Thermal Ionization Isotope Mass Spectrometer (TIMS), and the instrument model was Triton Ti. The process involved weighing 150 mg of the sample, dissolving it with deionized water, and centrifuging to remove the insoluble matter to eliminate the influence of other minerals. The Rb and Sr content of the samples were measured with the atomic absorption spectrometer (AAS); we weighed 1g of the sample, dissolved in deionized water and filtered to remove insolubles. The $^{87}Sr/^{86}Sr$ measured by the international standard NBS-987 is 0.710266with a 2σ uncertainty of ± 0.000007 (external precision).

4. Results

The analysis results of 16 carbon and oxygen isotopes and the corresponding Mn and Sr contents are shown in Table 1. The $\delta^{13}C$ values of the upper Paleocene micritic dolomite are positive, and the variation range of the values is small, with values ranging from 4.2‰ to 5.7‰ (mean 5.3‰, S.D. = 0.4, $n = 9$). The $\delta^{18}O$ values vary widely, ranging from −5.2‰ to 2.4‰ (mean −1.7‰, S.D. = 2.5, $n = 9$). The variation in the $\delta^{13}C$ values of the lower Eocene micritic limestone is large, ranging from -6.9‰ to −2.0‰ (mean −5.3‰, S.D. = 1.9, $n = 7$); the $\delta^{18}O$ values vary widely, ranging from −9.0‰ to −6.4‰ (mean = −7.3‰, S.D. = 1.0, $n = 7$).

Table 1. Carbon and oxygen isotope compositions and related data for carbonate rocks from the upper Paleocene and lower Eocene strata in the Kuqa Depression.

Series	Lithology	Sample Number	$\delta^{13}C$ (PDB, ‰)	$\delta^{18}O$ (PDB, ‰)	Z Values	Mn/Sr	Remarks
Lower Eocene	micritic limestone	XKZB-01	−6.6	−8.5	109.55	0.93	
		XKZB-02	−6.9	−8.5	108.94	0.48	
		XKZB-03	−6.0	−6.4	111.82	2.44	
		XKZB-04	−5.4	−6.9	112.80	0.45	
		XKZB-05	−6.4	−9.0	109.71	0.36	
		XKZB-06	−2.0	−7.4	119.52	1.24	
		XKZB-07	−2.1	−7.0	119.51	0.87	
Upper Paleocene	micritic dolomite	TLK-01	5.7	0.2	139.07	1.85	
		TLK-02	5.5	0.4	138.76	0.17	
		TLK-03	5.2	−4.3	135.81	0.36	
		TLK-04	5.5	−5.2	135.97	0.32	
		TLK-05	5.4	−3.9	136.42	13.36	exclude
		TLK-06	5.3	−4.0	136.16	13.49	exclude
		TLK-07	4.2	2.4	137.10	6.28	exclude
		TLK-08	5.5	−0.1	138.51	2.10	
		TLK-09	5.3	−0.5	137.91	1.37	

The results from the analysis of 17 sulfur isotopes and 11 strontium isotopes are shown in Table 2. The variation in the $\delta^{34}S$ values of the upper Paleocene gypsum is very small, with values ranging

from 16.5‰ to 17.9‰ and an average of 17.3‰. The $\delta^{34}S$ values of lower Eocene gypsum vary widely, ranging from 10.5‰ to 17.0‰, with an average of 13.2‰; the $^{87}Sr/^{86}Sr$ ratios of the gypsum range from 0.708642 to 0.709883, with an average of 0.709184.

Table 2. Sulfur and strontium isotopic compositions of gypsum from the upper Paleocene and lower Eocene strata in the Kuqa Depression.

Series	Lithology	Sample Number	$\delta^{34}S$ (‰)	$^{87}Sr/^{86}Sr$
Lower Eocene	gypsum	XKZB-S01	17.0	0.708642 ± 11
		XKZB-S02	15.7	0.708929 ± 9
		XKZB-S03	14.4	0.709017 ± 6
		XKZB-S04	12.2	0.709062 ± 7
		XKZB-S05	14.1	0.709060 ± 7
		XKZB-S06	15.1	0.709193 ± 10
		XKZB-S07	11.1	0.709495 ± 12
		XKZB-S08	10.6	0.709494 ± 8
		XKZB-S09	10.8	0.709252 ± 6
		XKZB-S10	10.5	0.709883 ± 8
		XKZB-S11	13.3	0.709002 ± 7
Upper Paleocene	gypsum	TLK-S01	17.9	
		TLK-S02	17.8	
		TLK-S03	17.3	
		TLK-S04	17.2	
		TLK-S05	17.2	
		TLK-S06	16.5	

5. Discussion

5.1. Significance of the Carbon and Oxygen Isotopic Geochemistry

5.1.1. Validity of the Data

When using carbon and oxygen isotopes of carbonate rocks from marine strata to study the paleoenvironment, it is first necessary to determine if the samples are primary [32,33]. Carbonate rocks may undergo a series of alterations in the process of diagenesis and postdiagenesis that alter the original isotopic compositions, such as the effect of diagenetic fluids (especially atmospheric precipitation), recrystallization, and metamorphism. At present, to determine that the samples have not undergone diagenetic alteration, the following three conditions should be met: (1) In general, an Mn/Sr ratio of less than 3 is a criterion for determining the original carbon isotopic composition of a sample [34–36]; (2) It is generally believed that samples with $\delta^{18}O$ values less than −10‰ are altered and that the original information has been lost [35]; (3) A good correlation between the $\delta^{13}C$ values and the $\delta^{18}O$ values of carbonate rocks reflects the occurrence of strong diagenetic alteration, whereas a poor correlation reflects the occurrence of weak diagenetic alteration [37,38].

Three of the 16 samples have Mn/Sr ratios greater than 3 and are considered to exhibit nonprimary carbon isotopic compositions (Table 1). The $\delta^{18}O$ values of all samples were greater than −10‰ and could therefore be considered to be the original oxygen isotopic compositions. To eliminate the disturbance of diagenetic alteration, samples TLK-05, TLK-06, and TLK-07 were excluded, and the $\delta^{13}C$ and $\delta^{18}O$ values of the remaining samples were not significantly correlated (Figure 6a,b), with R^2 values of 0.1821 and 0.2252 for the Paleocene and Eocene rocks, respectively. Therefore, except for the

above three samples, the carbon and oxygen isotope data of the remaining samples reflect primary features and represent valid information.

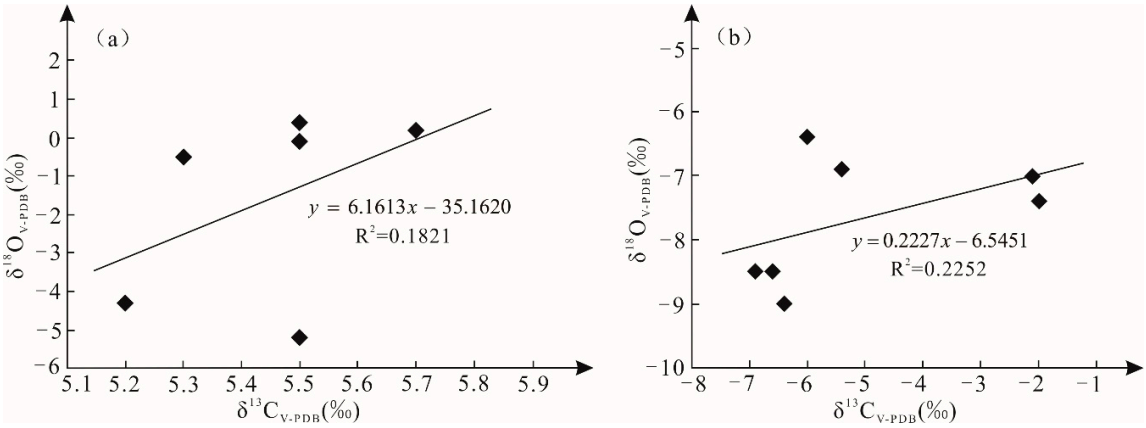

Figure 6. Correlations between $\delta^{13}C$ and $\delta^{18}O$ values of the upper Paleocene (**a**) and lower Eocene (**b**) carbonate rocks in the Kuqa Depression.

5.1.2. Upper Paleocene Carbonate Rocks

Having demonstrated that the samples retain primary information, we can determine the salinity of the diagenetic medium of the carbonate rocks based on the $\delta^{13}C$ values [39]. Keith and Weber (1964) [39] studied the carbon and oxygen isotopic compositions of limestone and calcium-bearing fossils. It is believed that $\delta^{13}C$ and $\delta^{18}O$ values can be used to determine the diagenetic medium salinity of carbonate rocks that formed before the Jurassic. When the salinity Z value ($Z = 2.048\ (\delta^{13}C_{PDB} + 50) + 0.498\ (\delta^{18}O_{PDB} + 50)$) is greater than 120, the carbonate formed under marine conditions; when the Z value is less than 120, the carbonate formed under freshwater conditions. The Z values of the Paleocene carbonate rocks range from 135.81 to 139.07, with an average of 137.67, all of which are much higher than 120, indicating a high salinity and stable marine sedimentary characteristics during formation of the carbonates.

The $\delta^{13}C$ values of the Talak Formation have a small variation range, whereas the $\delta^{18}O$ values vary widely. This may be because the carbon isotopic composition is more stable than the oxygen isotopic composition during diagenesis, so the carbon isotopic composition better reflects the original composition of the Tethyan seawater [40]. Figure 7 shows that the range of $\delta^{13}C$ values from the upper Paleocene carbonate rocks is very small and similar to the range of $\delta^{13}C$ values of marine carbonates. Furthermore, the range of values overlaps the range of $\delta^{13}C$ values of evaporation-produced carbonate. Therefore, the upper Paleocene carbonate rocks have seawater sedimentary features. The higher $\delta^{13}C$ values indicate that the ancient seawater did not receive freshwater replenishment with low carbon isotopic compositions, but it did experience a strong evaporation and concentration effect.

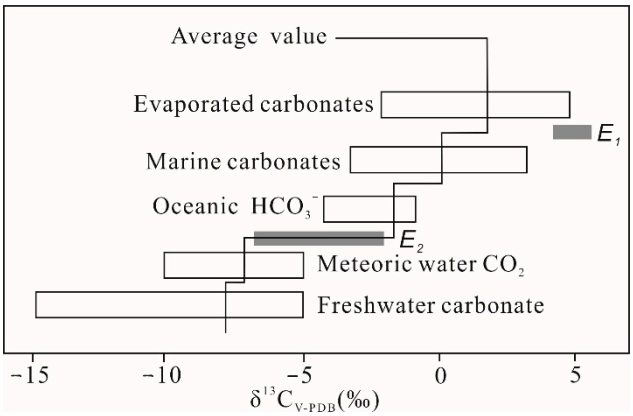

Figure 7. Distribution of carbon isotopic values in various carbonate rocks and related materials (modified from Schopf 1980 [41]). The gray bars E_1 and E_2 represent the distribution ranges of $\delta^{13}C$ values in the upper Paleocene and lower Eocene strata, respectively.

Cao et al. (2016) [42] noted that the Talak Formation of the Kuqa Depression formed in the same period as the upper Paleocene Aertashi Formation in the southwestern Tarim Basin. Bosboom et al. (2011; 2014) [27,43] found that Paleocene and Eocene Tethyan seawater simultaneously invaded the southwestern Tarim Basin and the Kuqa Depression from the west to the east through the Alay Valley. The above evidence indicates that the upper Paleocene salt-bearing strata in the southwestern Tarim Basin and the Kuqa Depression are products of the same era and are comparable. Previous studies on the carbon and oxygen isotopes of Paleocene marine carbonate rocks in the southwestern Tarim Basin show that the $\delta^{13}C$ values are positive (1.45~3.5‰) and the $\delta^{18}O$ values are negative (−5.9~−0.46‰) [44,45]. The distribution of oxygen isotopic values in the upper Paleocene carbonates is very similar to the previously published data, but the carbon isotopic values exhibit weak positive anomalies, which may be related to the burial of organic carbon by marine organisms within the strata [3].

5.1.3. Lower Eocene Carbonate Rocks

The main differences between the Xiaokuzibai Formation and the Talak Formation in terms of the carbon and oxygen isotopic compositions are that the former has significantly lower isotopic values than the latter (Figure 8) and that both $\delta^{13}C$ values and $\delta^{18}O$ values show negative bias characteristics. The range of measured $\delta^{13}C$ values overlaps with the range of $\delta^{13}C$ values for marine and freshwater carbonates (Figure 7), and the values tend to increase from the bottom of the section to the top, indicating that the input of terrestrial material enriched in the light isotope ^{12}C to the basin gradually decreased. The petrographic characteristics and salinity Z values of the carbonate samples are also consistent with this conclusion. The Z values of the lower Eocene carbonate rock range from 108.94 to 119.52 and increase significantly from the bottom of the section to the top. The above research results and petrographic characteristics of the carbonate rocks indicate that the bottom limestone deposits formed in a sedimentary environment with weak hydrodynamic conditions and the input of terrestrial debris upwards in the stratigraphy and then gradually transformed into an environment with less terrestrial debris input, possibly due to a transient increase in the supply of marine materials.

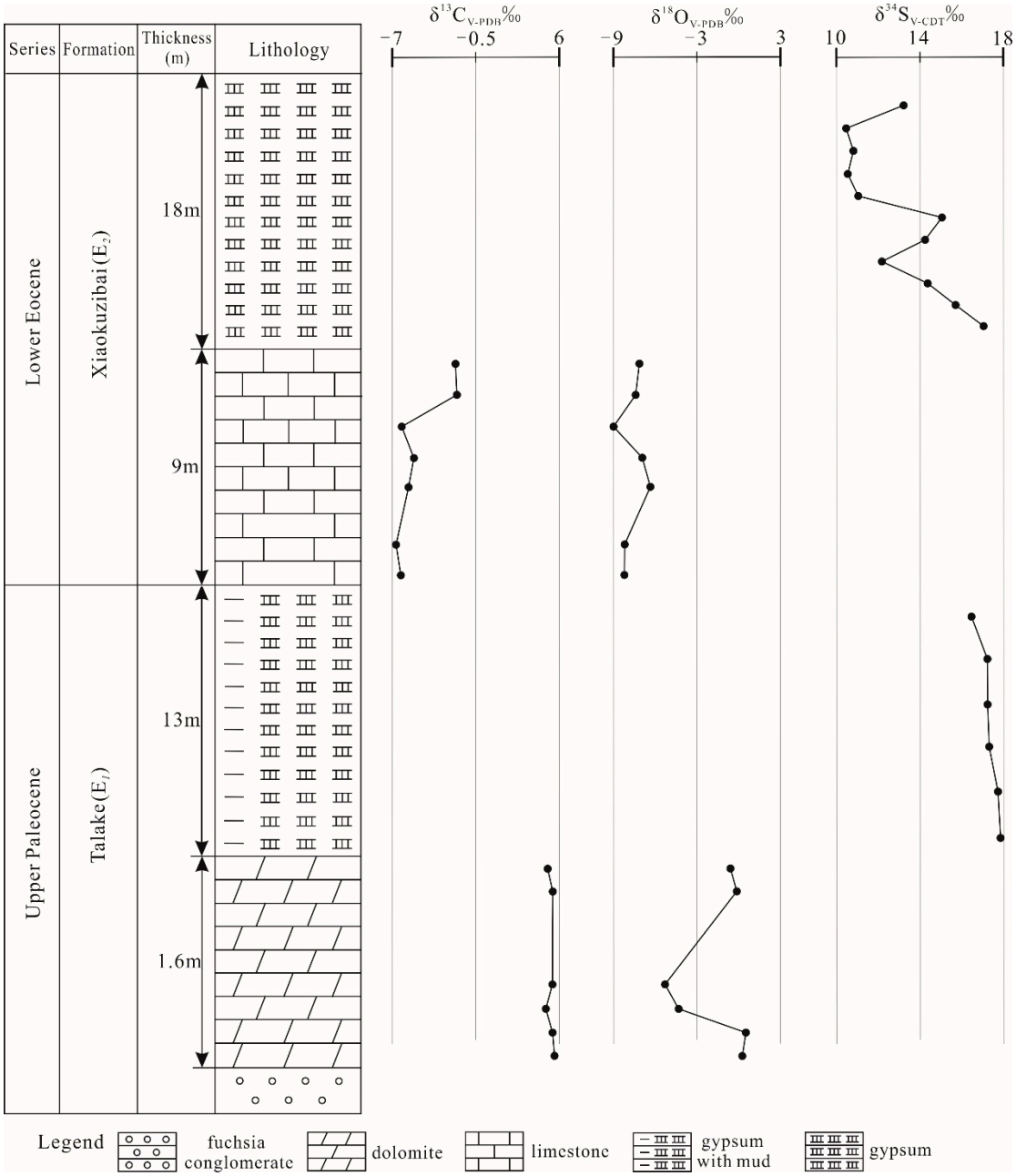

Figure 8. Lithology histogram of evaporite sequences in the upper Paleocene and lower Eocene strata, Kuqa Depression.

The carbon and oxygen isotopic trends are not related (Figure 6b), indicating an open sedimentary environment. A large amount of terrestrial material or freshwater enriched in the light isotope ^{12}C was frequently input into the basin during this period, resulting in low carbon isotopic values. The Paleocene and Eocene lithofacies paleogeographic features of the Kuqa Depression have been described [46]. The Paleocene Tethyan seawater first invaded the Kuqa Depression from the west, and the salt lake that formed was shallow. The Talak section was located on the western edge of the salt lake, which may be the reason why the carbonate rock layer in the Talak section is thin and the carbon and oxygen isotopic values are somewhat high. The salt lake was affected by intermittent transgressions, and the southern Tianshan mountain front and other sources provided terrigenous materials to the lake at the beginning of the Eocene, which led to further increases in the depth of

the salt lake and the area of the lake surface. This may explain the thick carbonate rocks and the low carbon and oxygen isotopic values in the Xiaokuzibai section.

5.2. Significance of the Sulfur Isotopic Geochemistry

The sulfur isotopic characteristics of sulfate minerals in evaporite basins are mainly affected by bacterial sulfate reduction, reservoir effects, and the composition of the source. Bacterial sulfate reduction causes the resulting sulfide to be significantly enriched in the light isotope ^{32}S, while the residual sulfate minerals are enriched in the heavy isotope ^{34}S [47]. For example, the $\delta^{34}S$ values of Early Triassic marine gypsum in the Sichuan Basin range from 27.8‰ to 35.9‰ [48], and the $\delta^{34}S$ values of Paleogene continental gypsum in the Dongpu Depression range from 28‰ to 33‰ [49]. Reservoir effects can cause the $\delta^{34}S$ values of postdeposition gypsum in a stratigraphic sequence to be slightly less than those of gypsum prior to deposition [47,50]. Sources of the sulfur present in evaporites include marine, terrestrial, and volcanic sources. The $\delta^{34}S$ value of marine sulfur is similar to the $\delta^{34}S$ value of contemporary seawater, and its range is small. The $\delta^{34}S$ values of terrestrial and volcanic sulfur are obviously lower than that of contemporary seawater, and their ranges are larger [50,51].

The $\delta^{34}S$ values of the upper Paleocene and lower Eocene gypsum in the Kuqa Depression are generally low, which is in sharp contrast with the high $\delta^{34}S$ values formed under strongly reducing conditions, indicating that sulfur isotope fractionation was induced by bacteria in the process of sulfate formation in the Kuqa Depression. Moreover, the petrologic characteristics do not show the presence of sulfides or other minerals indicative of a reducing environment, and the widely developed red layer indicates that the depositional environment had a high redox potential, which would not have been conducive to the survival of sulfate-reducing bacteria. Therefore, it is inferred that the sulfate samples in this paper are not associated with bacterial reduction. Further supporting the lack of the effect of bacterial reduction on sulfur isotope fractionation, the $\delta^{34}S$ values of gypsum from the Talak section are rather high and feature a narrow range (16.5~17.9‰). These $\delta^{34}S$ values all fall within the same range as those of contemporary marine evaporites. Additionally, the $\delta^{34}S$ values of the strata decrease gradually from bottom to top, indicating that the reservoir effects or a small input of terrigenous materials may have played an important role in this variation. The above evidence indicates that these gypsum deposits formed in a marine sedimentary environment. However, the $\delta^{34}S$ values of the gypsum from the Xiaokuzibai Formation decrease to a greater degree, and most $\delta^{34}S$ values are lower than the $\delta^{34}S$ values of contemporary marine sulfate, indicating that the seawater was frequently affected by continental freshwater during the process of evaporation, which shows that the sedimentary environment gradually changed from marine to continental.

Zhang et al. (2013) and Sun (2014) [8,52] performed sulfur isotope analysis on gypsum samples from the Paleocene Artashi Formation collected from surface sections and drill wells and showed that the $\delta^{34}S$ values ranged from 16.6‰ to 20.6‰ and 16.4~19.1‰, respectively, exhibiting typical marine source characteristics. The sulfur isotope values of the gypsum from the upper Paleocene Talak section in the Kuqa Depression are similar and within these ranges. Therefore, the upper Paleocene gypsum deposits formed in a marine sedimentary environment, while the lower Eocene gypsum deposits formed in a sedimentary environment that gradually changed from marine to continental.

5.3. Significance of the Strontium Isotopic Geochemistry

Primary gypsum carries and usually retains the strontium isotopic composition of the water body from which the gypsum precipitated. The strontium isotopic ratio of marine gypsum is similar to the strontium isotopic ratio of the contemporary seawater, and the variation range is very small. The radioactive strontium isotopic ratio of continental gypsum is larger than the strontium isotopic ratio of contemporaneous seawater and plots far from the strontium isotope curve of contemporaneous seawater. For example, the $^{87}Sr/^{86}Sr$ ratio of Paleogene continental gypsum in the Dongpu Depression ranges from 0.7116 to 0.7137 [53]. The strontium isotopic ratio of gypsum from the sea-land transition phase is commonly affected by the mixing of seawater and terrestrial water and has the characteristics

of both. For example, the strontium isotope ratios of gypsum from a Jurassic marginal sea environment range from 0.70836 to 0.71174 [54], and the strontium isotope ratios of middle Miocene marine gypsum affected by terrestrial radioactive strontium range from 0.708873 to 0.709106 [9].

The strontium isotope ratio of gypsum samples from the Xiaokuzibai section has an increasing trend; the lowest ratio (0.708642) is higher than the strontium isotopic ratio of contemporaneous seawater (Figure 9b) and higher than the maximum strontium isotopic ratio of marine foraminifera from the Gamba area of Tibet in the Tethyan realm during the same period [55]. The strontium isotopic ratio of minerals in evaporites associated with seawater is higher than that of contemporaneous seawater, and such a difference is usually interpreted as the effect of secondary precipitation or the recrystallization of minerals under the action of radioactive ^{87}Sr-bearing fluids [55,56]. However, under the conditions of well-preserved primary fluid inclusions and X-ray diffraction microanalysis, the gypsum samples in this study have not experienced recrystallization. Therefore, the strontium isotopic signatures reflect a gradual increase in radiogenic Sr due to the constant input of nonmarine material during the gypsum formation period.

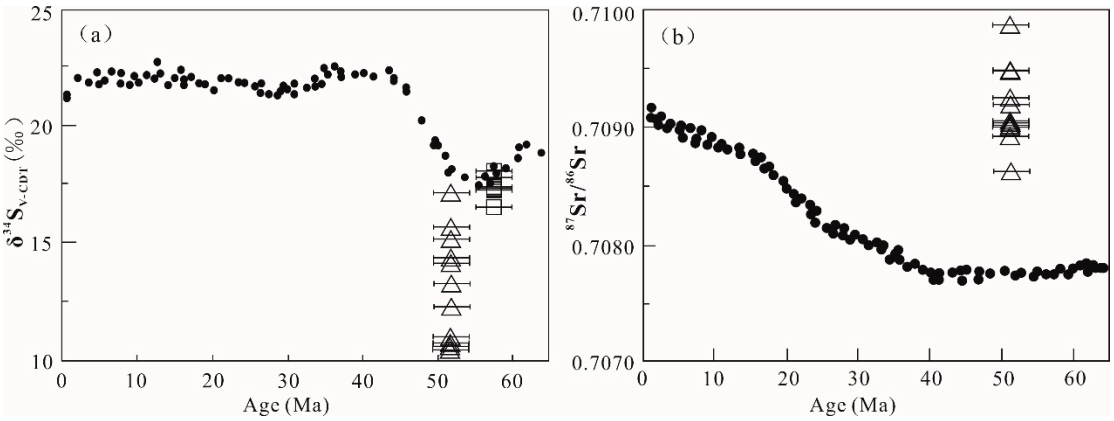

Figure 9. Plots of the δ^{34}S values (**a**) and ^{87}Sr/^{86}Sr ratios (**b**) of the Paleocene and Eocene gypsum in the Kuqa Depression and contemporaneous seawater. Squares represent the values of the Paleocene gypsum samples, and triangles represent the values of the Eocene gypsum samples. The δ^{34}S seawater curve is from Paytan et al. (1998) [57]. The ^{87}Sr/^{86}Sr seawater curve is from McArthur et al. (2001) [58].

Our results are similar to the strontium isotopic ratios (0.708718~0.709326) of Eocene marine-continental rock salt in the Kuqa Depression, as measured by Wang et al. (2015) [59], but they are clearly different from the strontium isotopic ratios (0.709909~0.710868) of Miocene continental rock salt in the Kuqa Depression. In addition, the strontium isotopic ratios have a good correlation with the sulfur isotopic values from the same samples (R^2 = 0.7, Figure 10), indicating that the source of the sulfur was related to the source of the strontium (calcium) in the gypsum and that the sulfur and strontium isotopic characteristics are a result of mixing between marine and continental materials. Therefore, the continuous mixing of terrestrial materials was the main factor causing sulfur isotopic values and strontium isotopic ratios to gradually move away from the isotopic values of contemporaneous seawater.

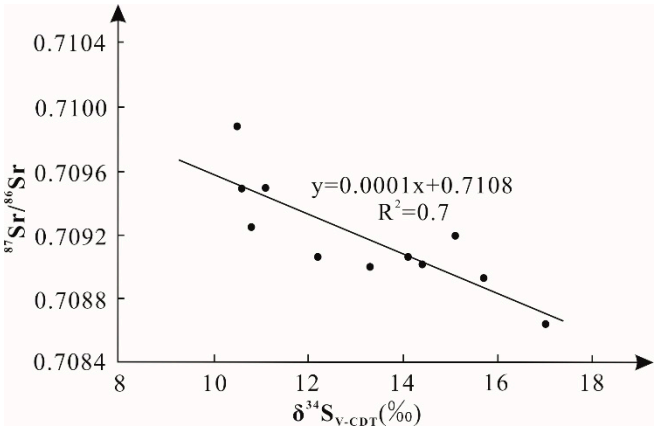

Figure 10. Correlation between sulfur and strontium isotopic compositions within the gypsum in the lower Eocene strata of the Kuqa Depression.

6. Conclusions

The petrologic characteristics of the studied carbonate rocks indicate that the Kuqa Depression featured a sedimentary environment characterized by weak hydrodynamic conditions and no terrigenous material input in the late Paleocene. Later, during the early Eocene, the sedimentary environment continued to feature weak hydrodynamic conditions, but the supply of terrigenous debris first increased and then decreased and disappeared. The carbon and oxygen isotopic compositions of carbonate rocks and the strontium isotopic compositions of gypsum rocks show that the Kuqa Depression experienced a Tethys transgression in the Late Paleocene. In contrast, the Tethys retreated during the early Eocene, began to accept continental deposits, and then experienced a transient transgression. Finally, it gradually evolved into continental deposits (Figure 11). The isotope geochemistry characteristics are consistent with the petrographic characteristics of carbonate rocks.

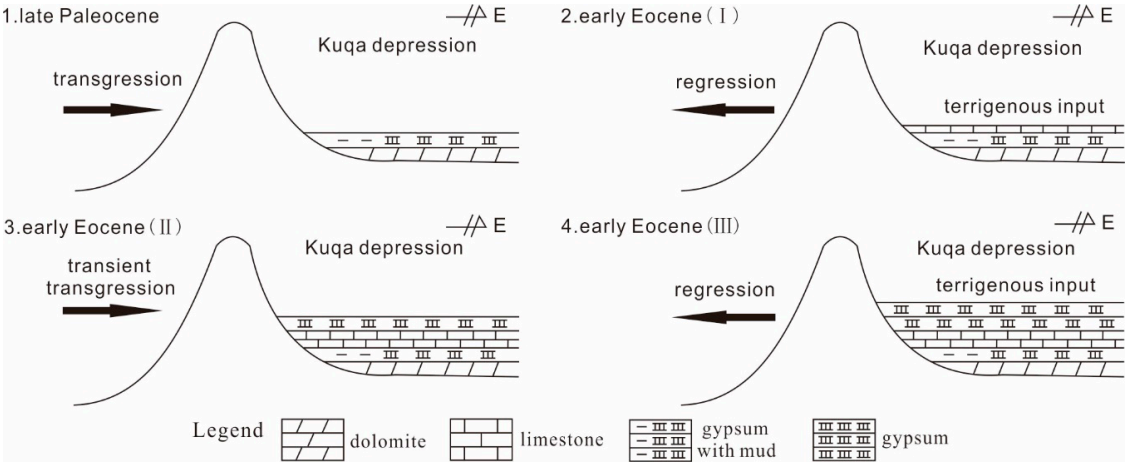

Figure 11. Evolution of late Paleocene-early Eocene transgressions in the Kuqa Depression.

Author Contributions: Y.X. performed the data analyses and wrote the manuscript; Y.C. helped perform the analysis with constructive discussions; C.L. contributed to the conception of the study and editing; H.Z. and X.N. performed the experiment; All authors have read and agreed to the published version of the manuscript.

Funding: This study was supported by the Basic Research Project for the Central Public Welfare Scientific Institutions (YYWF201716) granted by the Institute of Mineral Resources Chinese Academy of Geological Sciences and National Natural Science Foundation of China (No. 41902064 and No. 41602100).

Acknowledgments: We especially thank the Editor-in-Chief and anonymous reviewers for constructive comments and suggestions that have greatly improved the quality of this manuscript.

Conflicts of Interest: The authors declare no conflict of interest.

References

1. Abels, H.A.; Dupont-Nivet, G.; Xiao, G.; Bosboom, R.; Krijgsman, W. Step-wise change of Asian interior climate preceding the Eocene-Oligocene Transition (EOT). *Palaeogeogr. Palaeoclim. Palaeoecol.* **2011**, *299*, 399–412. [CrossRef]
2. Wang, H.Z. *Paleogeophic Atlas of China*; China Cartographic Publishing House: Beijing, China, 1985.
3. Su, X.; Guo, X.P.; Ding, X.Z. Late Cretaceous and Paleocene calcareous nannofossil assemblages from Kuche foreland Basin in the Northern Tarim Basin. *Geoscience* **2003**, *17*, 370–377.
4. Zhu, Y.H.; Zhao, Y.Y.; Zhong, S.L. Paleogene calcareous nannofossil from the Xiaokuzibai section of the Kuqa depression, Tarim Basin. *Acta Palaeontol. Sin.* **2012**, *51*, 328–333.
5. Fu, Q.L. Relationships between carbon and oxygen isotopic compositions and diagenetic environments of Lower Tertiary carbonate on the northwestern margin of Kuqa Basin, Xinjiang. *J. Stratigr.* **1996**, *4*, 280–284.
6. Jia, J.H. Carbonate rocks and their genetic significance of the Mesozoic and Cenozoic in Kuqa depression of Xinjiang area. *J. Paleogeography* **2002**, *4*, 30–38.
7. Liu, Q. *Mesozoic and Cenozoic Terrigenous Clastic Rocks Chemical Sedimentary Rocks in China*; Beijing Science and Technology Press: Beijing, China, 1987; pp. 15–17.
8. Zhang, H.; Liu, C.L.; Cao, Y.T.; Sun, H.W.; Wang, L.C. A tentative discussion on the time and the way of marine regression from Tarim Bay during the Cenozoic. *Acta Geosci. Sin.* **2013**, *34*, 577–584.
9. Cendon, D.I.; Peryt, T.M.; Ayora, C.; Pueyo, J.J.; Taberner, C. The importance of recycling processes in the Middle Miocene Badenian evaporite basin (Carpathian foredeep): Palaeoenvironmental implications. *Palaeogeogr. Palaeoclim. Palaeoecol.* **2004**, *212*, 141–158. [CrossRef]
10. Playà, E.; Cendón, D.I.; Travé, A.; Chivas, A.R.; García, A. Non-marine evaporites with both inherited marine and continental signatures: The Gulf of Carpentaria, Australia, at ~70 ka. *Sediment. Geol.* **2007**, *201*, 267–285. [CrossRef]
11. Zhang, Q.Y.; Liang, B.; Qin, F.R.; Cao, J.W.; Dan, Y.; Li, J.R. Environmental and geochemical significance of carbon and oxygen isotopes of Ordovician carbonate paleokarst in Lunnan, Tarim Basin. *Environ. Earth Sci.* **2016**, *75*, 1074.
12. Tabakh, M.E.; Utha-Aroon, C.; Schreiber, B.C. Sedimentology of the Cretaceous Maha Sarakham evaporites in the Khorat Plateau of northeastern Thailand. *Sediment. Geol.* **1999**, *123*, 31–62. [CrossRef]
13. Playà, E.; Ortí, F.; Rosell, L. Marine to non-marine sedimentation in the upper Miocene evaporites of the Eastern Betics, SE Spain: Sedimentological and geochemical evidence. *Sediment. Geol.* **2000**, *133*, 135–166. [CrossRef]
14. Kelts, K. Lacaustrine Basin Analysis and Correlation by Strontium Isotope Stratigraphy. In *Abstract of 13th International Sedimentary*; Nottingham University: Nottingham, UK, 1987; pp. 9–13.
15. Flecker, R.; Villiers, S.D.; Ellam, R.M. Modelling the effect of evaporation on the salinity 87Sr/86Sr relationship in modern and ancient marginal-marine systems: The Mediterranean Messinian Salinity Crisis. *Earth Planet. Sci. Lett.* **2002**, *203*, 221–233. [CrossRef]
16. Palmer, M.R.; Cahit, H.; Fallick, A.E. Sulphur, sulphate oxygen and strontium isotope composition of Cenozoic Turkish evaporites. *Chem. Geol.* **2004**, *209*, 341–356. [CrossRef]
17. Alonso-Azcárate, J.; Bottrell, S.H.; Mas, J.R. Synsedimentary versus metamorphic control of S, O and Sr isotopic compositions in gypsum evaporites from the Cameros Basin, Spain. *Chem. Geol.* **2006**, *234*, 45–57. [CrossRef]
18. Peryt, T.M.; Anczkiewicz, R. Strontium isotope composition of Middle Miocene primary gypsum (Badenian of the Polish Carpathian Foredeep Basin): Evidence for continual non-marine inflow of radiogenic strontium into evaporite basin. *Terra Nova* **2015**, *27*, 54–61. [CrossRef]
19. Lu, H.F.; Howell, D.G.; Jia, D.; Cai, D.S.; Wu, S.M.; Chen, C.M.; Valin, Z.C.; Shi, Y.S. Rejuvenation of the Kuqa Foreland Basin, northern flank of the Tarim Basin, Northwest China. *Int. Geol. Rev.* **1994**, *36*, 1151–1158.
20. Zhang, C.J.; Tian, Z.Y. Tertiary salt structures and hydrocarbons in Kuqa depression of Tarim Basin. *Acta Pet Sin.* **1998**, *19*, 6–11.
21. Xu, J.X.; Ma, H.Z.; Yang, L.S.; Tan, H.B.; Wang, J.G. Paleaogene and Neogene tectonic environment and sedimentation of evaporite in Kuqa Basin. *Acta Geol. Sin.* **2006**, *80*, 227–235.

22. Cao, Y.T.; Yang, H.J.; Liu, C.L.; Gu, Q.Y.; Jiao, P.C.; Lu, Y.H. Response on sediment of evaporate in Kuqa Basin from Paleogene to Neogene period and Himalayan tectonic phase. *Acta Sedimentol. Sin.* **2010**, *28*, 1054–1065.
23. Burtman, V.S. Cenozoic crustal shortening between the Pamir and Tien Shan and a reconstruction of the Pamir-Tien Shan transition zone for the Cretaceous and Palaeogene. *Tectonophysics* **2000**, *319*, 69–92. [CrossRef]
24. Carrapa, B.; DeCelles, P.G.; Wang, X.; Clementz, M.K.; Mancin, N.; Stoica, M.; Kraatz, B.; Meng, J.; Abdulov, S.; Chen, F.H. Tectono-climatic implications of Eocene Paratethys regression in the Tajik basin of central Asia. *Earth Planet. Sci. Lett.* **2015**, *424*, 168–178. [CrossRef]
25. Chen, X.W.; Chen, H.L.; Lin, X.B.; Cheng, X.G.; Yang, R.; Ding, W.W.; Gong, J.F.; Wu, L.; Zhang, F.Q.; Chen, S.Q.; et al. Arcuate Pamir in the Paleogene? Insights from a review of stratigraphy and sedimentology of the basin fills in the foreland of NE Chinese Pamir, western Tarim Basin. *Earth Sci. Rev.* **2018**, *180*, 1–16. [CrossRef]
26. Zheng, H.B.; Tada, R.; Jia, J.T.; Lawrence, C.; Wang, K. *Cenozoic Sediments in the Southern Tarim Basin: Implications for the Uplift of Northern Tibet and Evolution of the Taklimakan Desert*; Geological Society, Special Publications: London, UK, 2010; Volume 342, pp. 67–78.
27. Bosboom, R.; Dupontnivet, G.; Grothe, A.; Brinkhuis, H.; Villa, G.; Mandic, O.; Stoica, M.; Huang, W.; Yang, W.; Guo, Z.; et al. Linking Tarim Basin sea retreat (west China) and Asian aridification in the late Eocene. *Basin Res.* **2014**, *26*, 621–640. [CrossRef]
28. Sun, J.M.; Windley, B.F.; Zhang, Z.L.; Fu, B.H.; Li, S.H. Diachronous seawater retreat from the southwestern margin of the Tarim Basin in the late Eocene. *J. Asian Earth Sci.* **2016**, *116*, 222–231. [CrossRef]
29. Zheng, M.; Meng, Z.F. Magnetostratigraphy of tertiary system in Baicheng, Xinjiang. *Acta Sedimentol. Sin.* **2006**, *24*, 650–656.
30. Teng, Z.H.; Yue, L.P.; He, D.F.; Deng, X.Q.; Bian, X.W. Magnetostratigraphic research of Cenozoic section of Kuche River area, South Xinjiang. *J. Stratigr.* **1997**, *21*, 55–62.
31. Goldstein, R.H.; Reynolds, T.J. Systematics of Fluid Inclusions in Diagenetic Minerals. *SEPM Short Course* **1994**, *31*, 155–199.
32. Drummond, C.N.; Patterson, W.P.; Walker, J.C.G. Climatic forcing of carbon-oxygen isotopic covariance in temperate-region marl lakes. *Geology* **1995**, *23*, 1031–1034. [CrossRef]
33. Leng, M.J.; Marshall, J.D. Palaeoclimate interpretation of stable isotope data from lake sediment archives. *Quat. Sci. Rev.* **2004**, *23*, 811–831. [CrossRef]
34. Veizer, J. Chemical diagenesis of carbonates: Theory and application of trace element technique. *Stable Isot. Sediment. Geol.* **1983**, *10*, 3–100.
35. Kaufman, A.J.; Knoll, A.H. Neoproterozoic variations in the C-isotopic composition of seawater: Stratigraphic and biogeochemical implications. *Precambrian Res.* **1995**, *73*, 27–49. [CrossRef]
36. Nan, J.Y.; Liu, Y.Y. Organic and inorganic carbon-isotope shift and paleoenvironment at the P-T boundary section in Meishan, Zhejiang Province. *Geochimica* **2004**, *33*, 9–19.
37. Qing, H.R.; Veizer, J. Oxygen and carbon isotopic composition of Ordovician brachiopods: Implications for coeval seawater. *Geochim. Cosmochim. Acta* **1994**, *58*, 4429–4442. [CrossRef]
38. Veizer, J.; Ala, D.; Azmy, K.; Bruckschen, P.; Buhl, D.; Bruhn, F.; Carden, G.A.; Diener, A.; Ebneth, S.; Godderis, Y.; et al. 87Sr/86Sr, δ13C and δ18O evolution of Phanerozoic seawater. *Chem. Geol.* **1999**, *161*, 1586. [CrossRef]
39. Keitht, M.H.; Weber, J.N. Carbon and oxygen stable isotopic composition of selected limestones and fossils. *Geochim. Cosmochim. Acta* **1964**, *28*, 1787–1816. [CrossRef]
40. Muttoni, G.; Mazza, M.; Mosher, D.; Katza, M.E.; Kent, D.V.; Balini, M. A Middle-Late Triasic (Ladinian-Rhaetian) carbon and oxygen isotope record from the Tethyan Ocean. *Palaeogeogr. Palaeoclim. Palaeoecol.* **2014**, *399*, 246–259. [CrossRef]
41. Schopf, T.J.M. *Paleoceanography*; Harvard University Press: Cambridge, MA, USA, 1980.
42. Cao, Y.T.; Liu, C.L.; Yan, H.; Jiao, P.C.; Zhang, H.; Lü, F.L.; Ding, T. Research on evaporite deposit and its controlling factors for saline lake chain of Tarim Basin and central Asia basin during Mesozoic-Cenozoic period. *Miner. Depos.* **2016**, *35*, 591–604.
43. Bosboom, R.E.; Dupont-Nivet, G.; Houben, A.J.P.; Brinkhuis, H.; Villa, G.; Mandic, O.; Stoica, M.; Zachariasse, W.J.; Guo, Z.; Li, C. Late Eocene sea retreat from the Tarim Basin (west China) and concomitant Asian paleoenvironmental change. *Palaeogeogr. Palaeoclim. Palaeoecol.* **2011**, *299*, 385–398. [CrossRef]

44. Guo, X.P. Study on marine Cretaceous-Tertiary boundary in the Western Tarim Basin. *Earth Sci.* **1990**, *3*, 325–335.
45. Li, B.Y.; Zhou, Y.Q.; Wu, S.Z.; Li, Y.A. Characteristics of carbon and oxygen isotope of limestone from Yigeziya and Kalataer formations in southwestern Tarim Basin. *Xinjiang Geol.* **2002**, *20*, 88–90.
46. Liu, C.L.; Cao, Y.T.; Yang, H.J.; Jiao, P.C.; Gu, Q.Y. Discussion on Paleogene-Neogene environment change of salt lakes in Kuqa Foreland Basin and its potash-forming effect. *Acta Geosci. Sin.* **2013**, *34*, 547–558.
47. Strauss, H. Geological evolution from isotope proxy signals—Sulfur. *Chem. Geol.* **1999**, *161*, 89–101. [CrossRef]
48. Lin, Y.T. Study on sulfur isotope of Trias marine deposit gypsum and brines in the Sichuan Basin. *J. Saltlake Res.* **2003**, *11*, 1–7.
49. Shi, Z.S.; Chen, K.Y.; He, S. Strontium, sulfur and oxygen isotopic compositions and significance of paleoenvironment of Paleogene of Dongpu depression. *Earth Sci.* **2005**, *30*, 430–436.
50. Holser, W.T.; Kaplan, I.R. Isotope geochemistry of sedimentary sulfates. *Chem. Geol.* **1966**, *1*, 93–135. [CrossRef]
51. Toulkeridis, T.; Podwojewski, P.; Clauer, N. Tracing the source of gypsum in New Caledonian soils by REE contents and S-Sr isotopic compositions. *Chem. Geol.* **1998**, *145*, 61–71. [CrossRef]
52. Sun, H.W. *Sedimentary Characteristics of the Cretaceous-Paleogene Evaporates in Yarkand Basin, Xinjiang Northwestern China and Implication for Potash Information*; China University of Geosciences (Beijing): Beijing, China, 2014; pp. 66–67.
53. Leybourne, M.I.; Denison, R.E.; Cousens, B.L.; Bezys, R.K.; Gregoire, D.C.; Boyle, D.R.; Dobrzanski, E. Geochemistry, geology, and isotopic (Sr, S, and B) composition of evaporites in the Lake St. Martin impact structure: New constraints on the age of melt rock formation. *Geochem. Geophys. Geosystems* **2007**, *8*. [CrossRef]
54. Wan, X.Q.; Wang, X.; Yu, T.; Li, G.B. The global Paleocene/Eocene Thermal Maximum event in the Gamba area, Tibet. *Earth Sci. Front.* **2006**, *13*, 218–226.
55. Chaudhuri, S.; Clauer, N. *History of Marine Evaporites: Constraints from Radiogenic Isotopes//Isotopic Signatures and Sedimentary Records*; Springer: Berlin/Heidelberg, Germany, 1992; Volume 43, pp. 177–198.
56. Shields, G.A. A normalised seawater strontium isotope curve: Possible implications for Neoproterozoic-Cambrian weathering rates and the further oxygenation of the Earth. *Earth* **2007**, *2*, 35–42. [CrossRef]
57. Paytan, A.; Kastner, M.; Campbell, D.; Thiemens, M.H. Sulphur isotopic composition of Cenozoic seawater sulphate. *Science* **1998**, *282*, 1459–1462. [CrossRef]
58. McArthur, J.M.; Howarth, R.J.; Bailey, T.R. Strontium isotope stratigraphy: LOWESS version 3: Best fit to the marine Sr-isotope curve for 0–509 Ma and accompanying look-up table for deriving numerical age. *J. Geol.* **2001**, *109*, 155–170. [CrossRef]
59. Wang, X.Y.; Yin, H.W.; Deng, X.L.; Wei, Z. Strontium isotope characteristics and the origin of Cenozoic salt deposits in Kuqa depression. *J. Nanjing Univ. (Nat. Sci.)* **2015**, *51*, 1068–1074.